ACCSCIENCE PUBLISHING

Materials Science in Additive Manufacturing

ORIGINAL RESEARCH ARTICLE

Sunflower-inspired composite metastructure for broadband microwave absorption fabricated via fused deposition modeling

Pengfei Fang[1,2], Fei Wang[1,2]*, Zhe Zhang[1,2], Kaiyong Jiang[1,2], and Peifeng Li[3]*

[1]Fujian Key Laboratory of Special Energy Manufacturing, Huaqiao University, Xiamen, Fujian, China
[2]Xiamen Key Laboratory of Digital Vision Measurement, Huaqiao University, Xiamen, Fujian, China
[3]James Watt School of Engineering, University of Glasgow, Glasgow, United Kingdom

Abstract

Microwave-absorbing structures are increasingly vital for applications such as electromagnetic protection, stealth technology, and wireless communications. However, their broader adoption is often limited by drawbacks such as excessive thickness, narrow absorption bandwidth, and high manufacturing costs. This study presents the design, fabrication, and evaluation of a sunflower-inspired metastructure for broadband microwave absorption, achieved via fused deposition modeling three-dimensional printing. The metastructure, inspired by the spiral geometry of sunflower seed arrangements, integrates multi-layered, gradient spiral elements composed of carbon black-carbonyl iron powder/polylactic acid (CB-CIP/PLA) composites. Electromagnetic simulations were employed to systematically optimize key structural parameters, including the gradient impedance increment and individual layer thicknesses, to maximize absorption efficiency. Both simulated and experimental results demonstrate that the absorber achieves an effective absorption bandwidth of 12.13 GHz (5.87 – 18.00 GHz) with reflection loss below 10 dB, covering the C, X, and Ku frequency bands. The performance is attributed to the synergistic effects of interfacial polarization and natural magnetic resonance within the CB-CIP/PLA composite. The metastructure also exhibits stable, wide-angle absorption properties, maintaining bandwidths exceeding 10 GHz for incident angles up to 50° under both transverse electric and transverse magnetic polarizations. The proposed sunflower-inspired design demonstrates significant advantages in bandwidth-to-thickness ratio, fabrication efficiency, and polarization insensitivity compared to conventional biomimetic absorbers. These findings highlight the promise of bio-inspired design strategies for developing lightweight, efficient, broadband microwave absorbers, providing valuable reference for future advancements in the field.

Keywords: Sunflower-inspired metastructure; Broadband microwave absorption; Composite metamaterial; 3D printing; Gradient impedance; Wide-angle absorption; Bio-inspired design

***Corresponding authors:**
Fei Wang
(wangfei@hqu.edu.cn)
Peifeng Li
(peifeng.li@glasgow.ac.uk)

Citation: Fang P, Wang F, Zhang Z, Jiang K, Li P. Sunflower-inspired composite metastructure for broadband microwave absorption fabricated via fused deposition modeling. *Mater Sci Add Manuf.* 2025;4(3):025220048.
doi: 10.36922/MSAM025220048

Received: May 31, 2025

Revised: June 16, 2025

Accepted: June 23, 2025

Published Online: August 1, 2025

1. Introduction

With the rapid advancement of electronic information technology and the widespread proliferation of electronic devices, electromagnetic radiation has emerged as a significant source of environmental pollution. Such radiation poses substantial risks in critical areas, including personal health care, military stealth, wireless communication, and environmental safety.[1-3] To mitigate these harmful effects, substantial research efforts have been directed toward developing effective microwave-absorbing materials. These materials typically include dielectric loss materials (e.g., MXene[4] and silicon nitride[5]), magnetic loss materials (e.g., ferrites[6] and metallic powders[7]), and conductive loss materials (e.g., carbon black,[8,9] graphene,[10] and carbon nanotubes[11]).

Traditional absorbing coatings exhibit strong adhesion to object surfaces; however, their intrinsic absorption properties are insufficient to achieve broadband electromagnetic wave absorption.[12-14] Consequently, it remains a significant challenge to develop absorbers simultaneously characterized by a broad bandwidth, lightweight, thin profile, and high structural strength. Achieving these attributes is essential for effectively reducing the reflection and scattering of electromagnetic waves across a broad frequency range.

To address these challenges, biomimetic approaches have become increasingly attractive by leveraging structural and functional inspirations from nature. Many organisms have evolved intricate surface microstructures capable of manipulating electromagnetic waves, offering potential solutions for advanced absorber designs.[15] Examples include algae,[16] bamboos,[17] moth eyes,[18] honeycombs,[19] butterfly wings (e.g., *Pachliopta aristolochiae*),[20] and corals.[21] Through detailed examination of these natural structures, researchers have successfully translated biological principles into effective microwave-absorbing metastructures. For example, inspired by the gyroidal microstructures on butterfly wings, An *et al.*[22] designed a bionic metastructure, achieving ultra-wide absorption bandwidth and exhibiting stable microwave absorption even at an incident angle of 60°, despite the total thickness reaching 15 mm. Similarly, Chen *et al.*[23] fabricated a moth-eye-inspired microwave absorber using conductive graphite powder, resulting in an effective absorption bandwidth (EAB) of 13 GHz across the C, X, and Ku bands. However, this design required a relatively thick structure of 20 mm. Plant-inspired designs have also been explored. For example, Chen *et al.*[24] developed a layered aerogel based on liquid metal MXene, drawing inspiration from plant structures. This design achieved a maximum reflection loss (RL) of −73.2 dB at a density of 4.4 mg/cm^3, although with an EAB of only 7 GHz. Despite these advancements, considerable room remains for optimizing designs to achieve broader bandwidths, lighter weight, and thinner structures.

Among numerous biological templates, the sunflower exhibits a particularly promising structural geometry for bio-inspired engineering applications. Sunflower petals have inspired novel solar collectors integrating pulsating heat pipes into flat-plate designs.[25] Besides, sunflower stem pith is identified as an ultra-lightweight porous structure exhibiting exceptional mechanical properties and energy absorption capabilities.[26] In addition, the spiral arrangement of sunflower heads has informed the design of efficient deployable structures utilizing flat-folded isogonal spiral patterns.[27]

Motivated by these unique characteristics, this study proposes a novel sunflower-inspired microwave-absorbing metastructure, fabricated from a carbon black-carbonyl iron powder/polylactic acid (CB-CIP/PLA) composite via fused deposition modeling (FDM). By mimicking the sunflower disk's spiral pattern, the proposed metastructure aims to achieve enhanced broadband microwave absorption performance, reduced structural thickness, and a simplified fabrication process. Experimental analyses and electromagnetic simulations confirmed excellent microwave absorption under wide-angle and varying polarization conditions. The insights gained from this research are expected to significantly advance the development and practical application of broadband microwave absorption materials, particularly in military stealth technology and wireless communication systems.

2. Methodology

2.1. Design of sunflower-inspired metastructure and electromagnetic simulation

The sunflower is characterized by a unique spiral arrangement of seeds in its flower head. The sunflower head exhibits two distinct sets of constant-velocity spirals, one rotating clockwise and the other counterclockwise, interwoven with each other (Figure 1A). This arrangement positions sunflower seeds at intersections of spirals, enabling dense packing with minimal spacing. Consequently, the sunflower head achieves stable and smooth growth from bracts to a large floral disk.

While sunflowers do not directly influence microwave absorption, their distinctive seed arrangement can inspire effective absorber designs. This seed pattern resembles a constant-velocity spiral (Figure 1B), which can be modeled in polar coordinates as follows:

$$R_i = k_i \times \theta_i \quad \text{(I)}$$

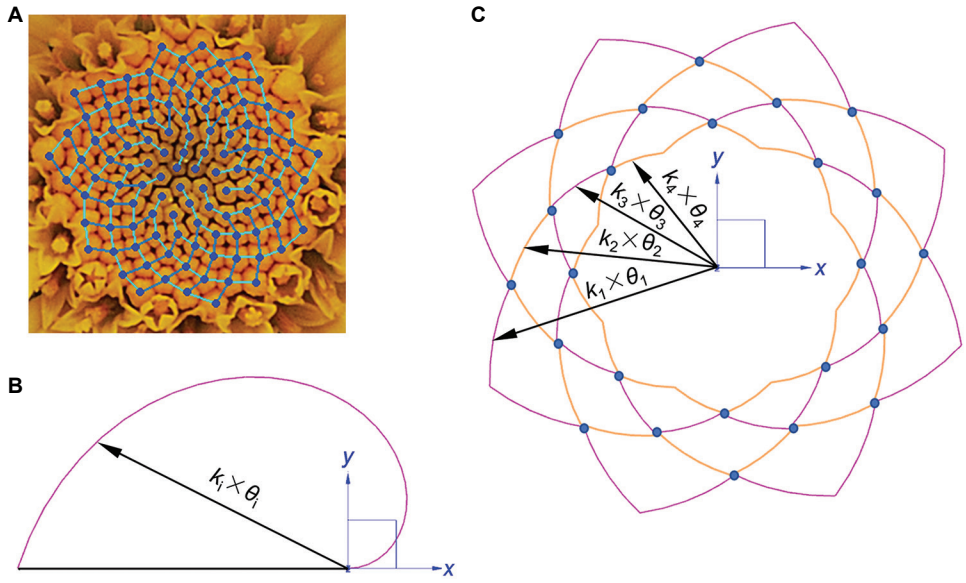

Figure 1. Modeling process for the sunflower-inspired metastructure. (A) Schematic representation of the spiral arrangement of seeds in a sunflower head, serving as the structural inspiration for the metastructure. (B) Outline of a single constant-velocity spiral. (C) Construction of mirrored and concentric spiral contours

where R_i represents the polar radius, θ_i is the polar angle, and k_i is the coefficient defining the spiral expansion rate. Figure 1C illustrates the modeling process of a sunflower-inspired spiral. Initially, the outermost spiral radius R_1 is determined by the periodic unit length L (equal to $2R$). Subsequent spirals are generated by performing mirror reflections (along the polar radius) and ring-array rotations (around the coordinate origin), progressively determining inner spiral intersections. This iterative process results in a gradient arrangement of spiral radii along the z-axis, producing a sunflower-like three-dimensional spiral structure in both clockwise and counterclockwise orientations.

A periodic array of these metastructure units is formed along the x and y directions (Figure 2A). Specific geometric parameters of the unit are detailed in Figure 2B. To achieve optimal electromagnetic performance, multiple spiral layers with distinct spiral coefficients (k_1, k_2, k_3, and k_4) are stacked vertically, creating a gradient distribution. Each spiral layer possesses an identical thickness (h_1=h_2=h_3=h_4). Electromagnetic simulations, including RL analysis and evaluations of electric, magnetic, and power loss field distributions, were performed using CST Studio Suite software (Dassault Systèmes, France).

2.2. Materials and fabrication

The raw materials used in this study included CB powder (surface area 55 – 70 m^2/g, resistivity 2.5 Ω·m) (Tianjin Zhengyuan Technology Co. Ltd., China), CIP powder (Hebei Lebo Metal Material Technology Co. Ltd., China),

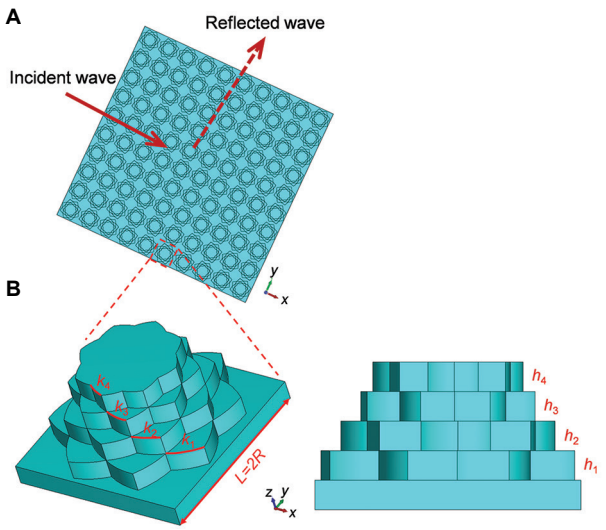

Figure 2. Structural characteristics of the sunflower-inspired metastructure. (A) Periodic array arrangement along the x and y axes. (B) A single metastructure unit cell illustrating key geometric parameters

and polymer matrix PLA powder (4032D) (Dongguan Huachuang Plastic Technology Co. Ltd., China). The sunflower-inspired metastructure was fabricated using FDM 3D printing (Figure 3). Before printing, CB-CIP/PLA composite filaments were prepared. First, CB and PLA were dried at 80°C for 6 h to remove residual moisture. Subsequently, PLA was mixed with 1.5 wt.% aluminate coupling agent, followed by the addition of 20 wt.% CB and 30 wt.% CIP. Note that the weight percentages here are relative to the PLA matrix mass. This mixture was

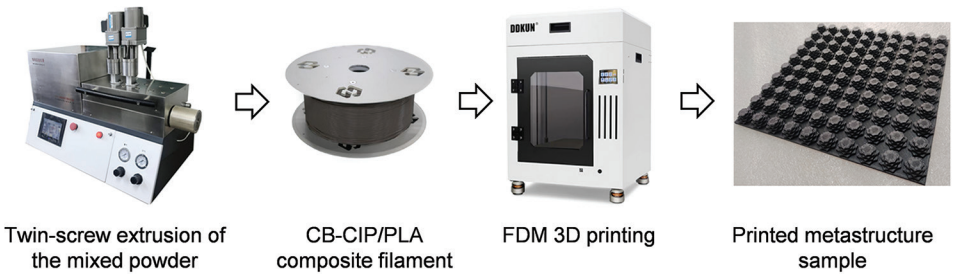

Figure 3. Fabrication of CB-CIP/PLA composite filaments and 3D printing process of the sunflower-inspired metastructure sample for microwave absorption testing
Abbreviations: CB-CIP/PLA: Carbon black-carbonyl iron powder/polylactic acid; FDM: Fused deposition modeling

homogenized using a dual-motion high-energy mixer (Zhengzhou Gold Co-Powder Technology Co. Ltd., China) with cylinder and blade speeds set at 28 rpm and 17 rpm, respectively, for 1 h. The uniformly mixed material was then fed into a micro twin-screw extruder (Wuhan Ruiming Experimental Instrument Manufacturing Co. Ltd., China) to produce filaments with a diameter of 1.75 ± 0.10 mm. The composite filaments were subsequently used to fabricate the designed metastructure through an FDM 3D printer (DDKUNT3040, Creative 3D Technology Co., Ltd., China) using the processing parameters as listed in Table 1. The printed metastructure sample (180 mm × 180 mm), composed of an array of 10 × 10 units, was finally prepared for microwave absorption testing.

2.3. Characterization and measurement

The microstructure of the fabricated composite was characterized using scanning electron microscopy (SEM). Electromagnetic parameters were measured in the frequency range of 2 – 18 GHz using a vector network analyzer (Keysight, USA) and adopting a coaxial transmission line method. Test specimens used for parameter measurements had an outer diameter of 7.00 mm, an inner diameter of 3.04 mm, and a thickness of 2.00 mm.

The microwave absorption performance of the printed metastructure was evaluated via a modified bow-shaped measurement method (Figure 4). Unlike the conventional bow-shaped method, where horn antennas and the sample are placed horizontally, this modified approach positions the horn antennas horizontally and the test sample vertically. Incident electromagnetic waves, transmitted from one horn antenna, are partially reflected off the sample surface. The reflected waves are either captured by the receiving antenna or absorbed by corner foam absorbers. This configuration enables precise measurement and analysis of microwave absorption performance across different incident angles and polarization states.

Table 1. Processing parameters in fused deposition modeling 3D printing

Parameter	Value
Printing speed (mm/s)	40
Layer height (mm)	0.2
Nozzle temperature (°C)	210
Bed temperature (°C)	50
Filling density (%)	100

3. Results and discussion

3.1. Morphology and electromagnetic properties of CB-CIP/PLA composite filaments

Figure 5A demonstrates the SEM image of the CB-CIP/PLA composite. The CB and CIP particles are largely uniformly dispersed within the PLA matrix, facilitated by high-temperature extrusion and frictional shear during twin-screw processing. However, due to the high specific surface area and surface energy of CB, agglomeration is observed. These CB agglomerates contribute to the formation of conductive networks, thereby enhancing the electrical conductivity and dielectric constant of the composite. Similarly, CIP particles, characterized by high surface activity, also show signs of localized agglomeration during the melting or molding process (as highlighted in Figure 5A). These CIP agglomerates increase local eddy current losses and suppress natural resonance behavior.[28] Note that the CB and CIP contents influence the microwave absorption performance of the filaments, with the combination of 20 wt.% CB and 30 wt.% CIP yielding the optimal absorption properties.[28] The electromagnetic parameters of the composite were characterized in the frequency range of 2 – 18 GHz. As shown in Figure 5B, the real and imaginary parts of the complex permittivity remain relatively stable across the measured frequency range. In contrast, both the real and imaginary components of the complex permeability exhibit a decreasing trend with increasing frequency.

To evaluate the microwave absorption performance of the composite, the RL was calculated for the composite absorber plate of varying thickness as follows:[29]

$$RL = 20\log\left|\frac{Z_{in} - Z_0}{Z_{in} + Z_0}\right| \quad \text{(II)}$$

$$Z_{in} = Z_0\sqrt{\frac{\mu}{\varepsilon}}\tanh\left[j\left(\frac{2\pi fd}{c}\right)\sqrt{\mu E}\right] \quad \text{(III)}$$

where Z_0, with a value of 377 Ω, is the impedance of free space, Z_{in} is the input impedance of the material, ε and μ are the relative complex permittivity and permeability, respectively, f is the frequency of the incident microwave, d is the thickness of the absorbing plate, and c, with a value of 3×10^8 m/s, is the speed of electromagnetic wave in free space.

Figure 6A and B present the RL curves and corresponding 3D plots, respectively, for composites of different thicknesses over the 2 – 18 GHz frequency range. As the thickness increases, the minimum RL (absorption peak) initially decreases and then increases, whereas the corresponding peak frequency shifts toward lower frequencies. This behavior is consistent with the quarter-wavelength ($\lambda/4$) matching condition,[30,31] which describes the relationship between matching thickness (d_m) and the peak matching frequency (f_m) as:

$$d_m = \frac{n\lambda}{4} = \frac{nc}{4f_m\sqrt{|\mu\varepsilon|}} \quad (n = 1,3,5,\ldots) \quad \text{(IV)}$$

where λ is the electromagnetic wavelength in the material.

Figure 6C demonstrates the experimental relationship between d_m and f_m. The red pentagrams denote the experimental matching points, which align closely with the theoretical $\lambda/4$ curve. This confirms the validity of the $\lambda/4$ model for the composite. However, the experimental points lie slightly above the theoretical curve, indicating that the absorption peaks occur at higher frequencies than predicted for a given thickness. This deviation is attributed to the intrinsic absorption properties of the material, which shift the peak absorption frequency. Meanwhile, Figure 6D illustrates the EABs (defined as RL < −10 dB) for thicknesses ranging from 1.5 to 4.0 mm. The widest EAB is achieved at a thickness of 2.0 mm, indicating that the absorption performance of the composite can be effectively tuned by adjusting the absorber plate thickness.

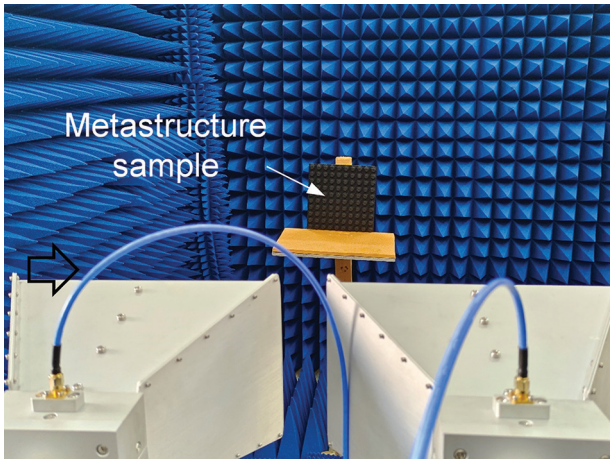

Figure 4. Experimental setup for microwave absorption measurements using the bow-shaped method, depicting the arrangement of the horn antennas and the sample positioning for reflection loss evaluation

3.2. Geometric optimization of the sunflower-inspired metastructure

3.2.1. Determination of spiral parameters

To achieve broadband microwave absorption, the geometric parameters of the sunflower-inspired metastructure were carefully investigated and optimized

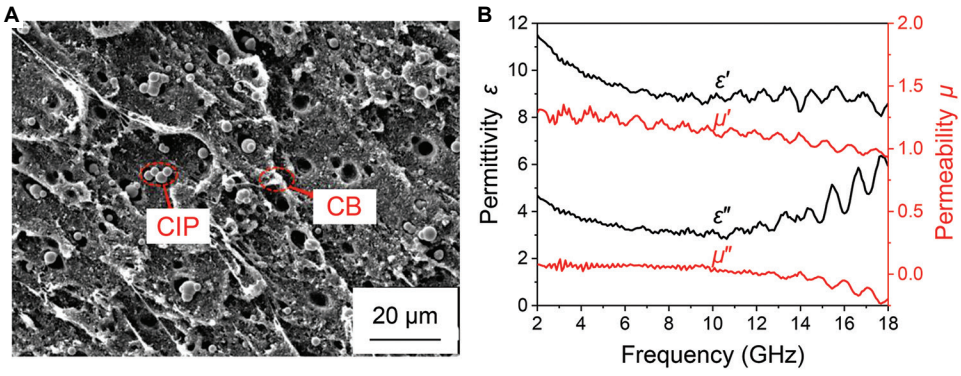

Figure 5. Morphology and electromagnetic properties of CB-CIP/PLA composite filaments. (A) SEM image of the composite, showing the dispersion and agglomeration of CB and CIP particles within the PLA matrix (scale bar: 20 μm; magnification: 1000×). (B) Real and imaginary parts of the composite's complex permittivity and permeability

Abbreviations: CB-CIP/PLA: Carbon black-carbonyl iron powder/polylactic acid; SEM: Scanning electron microscopy

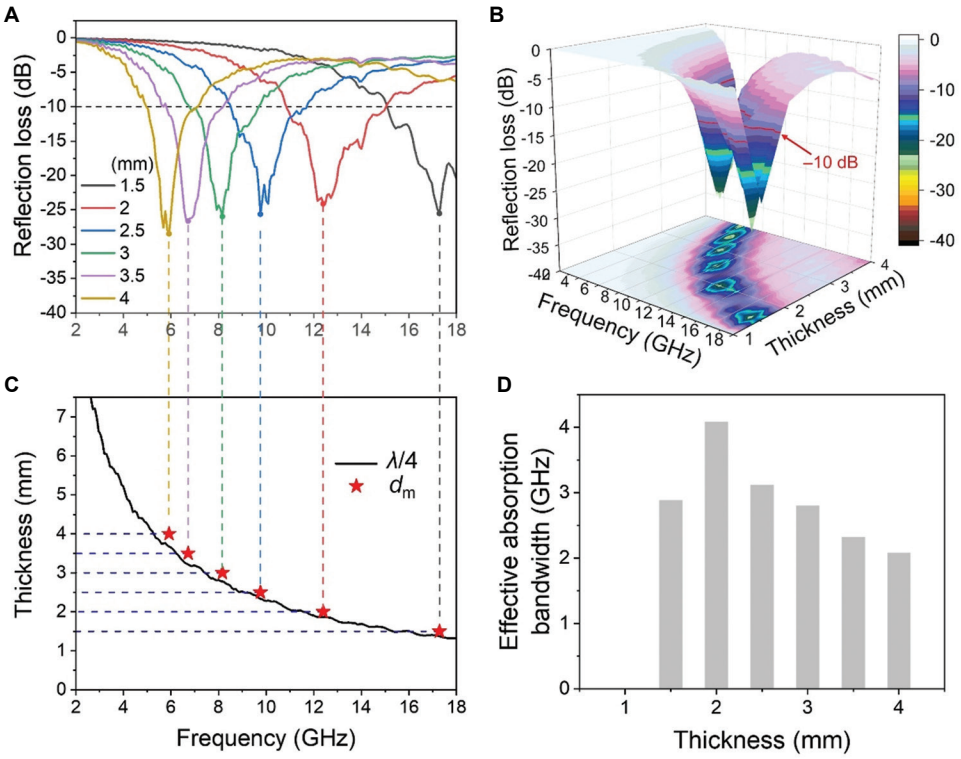

Figure 6. Microwave absorption performance of the CB-CIP/PLA composite. (A) Reflection loss curves for the composite at varying thicknesses over the 2 – 18 GHz frequency range. (B) A 3D representation of reflection loss versus frequency and sample thickness. (C) Relationship between matching thickness (d_m) and frequency (f_m), comparing the experimental data with the theoretical $\lambda/4$ model. (D) Effective absorption bandwidth as a function of sample thickness (1.0 – 4.0 mm)
Abbreviation: CB-CIP/PLA: Carbon black-carbonyl iron powder/polylactic acid

using electromagnetic simulations. The metastructure unit length (L) was set to 18 mm, and the polar radius of the constant-velocity spiral was thus determined as half the unit length (i.e., R = 9 mm) (Figure 2B). Based on the desired gradient characteristic impedance distribution, the parameters k (spiral coefficient) and θ (polar angle) of the constant-velocity spirals were calculated for each layer. The spiral layer thickness was fixed at $h_1 = h_2 = h_3 = h_4 = 2$ mm.

To ensure a smooth impedance gradient across the layers and achieve broadband impedance matching, the gradient impedance increment (ΔZ) between adjacent layers was varied systematically from 18 Ω to 28 Ω in steps of 2 Ω. The equivalent characteristic impedance (Z_i) of each layer was first calculated as follows:

$$Z_i = Z_0 \left| \sqrt{\frac{\mu_{eff}' - \mu_{eff}''}{\varepsilon_{eff}' - \varepsilon_{eff}''}} \right| \quad (V)$$

$$\Delta Z = Z_{i+1} - Z_i \quad (VI)$$

where ε_{eff} is the effective permittivity and μ_{eff} is the effective permeability. The impedance of the adjacent layer (Z_{i+1}) was then determined by controlling the ΔZ. The layers were sequentially stacked from bottom (closest to the metallic backplane) to top (closest to the air) in ascending order of impedance (Z_i). The bottom-most square layer featured a fixed characteristic impedance (Z) of 127.8 Ω. Next, the volume fraction f_c of each layer composed of constant-velocity spirals was calculated using the effective permittivity (ε_{eff}) and permeability (μ_{eff}):

$$\varepsilon_{eff} = \varepsilon f_c + (1 - f_c)\varepsilon_0 \quad (VII)$$

$$\mu_{eff} = \mu f_c + (1 - f_c)\mu_0 \quad (VIII)$$

where ε_c and μ_c represent the relative complex permittivity and permeability of the composite material, respectively, but ε_0 and μ_0 denote the respective values for air. The disk area S_i of each spiral layer was then obtained using the volume fraction f_c in Equation IX, and the spiral coefficient k_i for each layer was calculated using Equation X.

$$f_c = \frac{S_i}{L^2} \quad (IX)$$

$$S_i = 16 \times \int_{\frac{R_i}{k_i} - \frac{\pi}{8}}^{\frac{R_i}{k_i}} \frac{1}{2} k_i^2 \theta^2 d\theta \quad (X)$$

Figure 7 illustrates how the ΔZ influences the microwave absorption performance. With increasing ΔZ, the EAB for RL below −10 dB gradually decreases, whereas the EAB for RL below −15 dB initially increases and then decreases. Notably, when ΔZ reaches 24 Ω, the metastructure achieves an effective −10 dB absorption bandwidth of 14.07 GHz (3.93 – 18 GHz), covering the entire C, X, and Ku bands. In addition, the −15 dB absorption bandwidth reaches 11.54 GHz (4.25 – 5.15 GHz and 7.36 – 18 GHz). This enhanced performance at ΔZ of 24 Ω can be attributed to the reduced spiral coefficients (k_i), which intensify resonance interactions between adjacent layers, thus enabling efficient dissipation of microwave energy across a broad frequency range. However, further increasing ΔZ beyond 24 Ω (e.g., to 28 Ω) results in a narrowing of the EAB. Based on a comprehensive comparison of absorption bandwidth and RL performance, the optimal ΔZ was determined to be 24 Ω, with corresponding spiral coefficients k_1 of 4.39, k_2 of 2.80, k_3 of 2.74, and k_4 of 1.69.

3.2.2. Determination of layer thicknesses

Initially, the four gradient layers of the sunflower-inspired metastructure were equally divided without considering the influence of layer thickness on microwave absorption performance. To optimize the metastructure systematically, the individual thicknesses (h_1, h_2, h_3, and h_4) of each layer were analyzed separately using parametric sweeps in the CST software. During these sweeps, each layer thickness was varied independently from 1 to 3 mm in 0.5 mm increments, whereas the remaining layers were fixed at a baseline value of 2 mm.

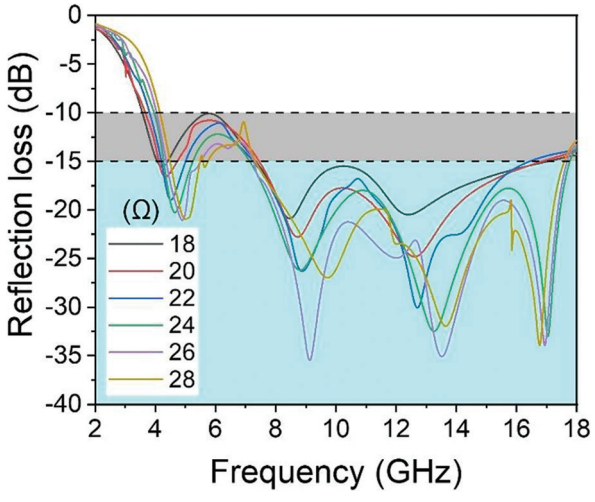

Figure 7. Effect of the gradient characteristic impedance increment (ΔZ) between adjacent layers on the absorption bandwidth and reflection loss of the sunflower-inspired metastructure

Figure 8 demonstrates how varying the thickness of each layer influences the metastructure's microwave absorption performance. Increasing either h_1 or h_2 shifts the low- and mid-frequency absorption peaks toward lower frequencies, while slightly shifting the high-frequency peak toward higher frequencies. In contrast, increasing h_3 or h_4 shifts low- and mid-frequency peaks to lower frequencies but does not notably affect the high-frequency peak position. Although these adjustments slightly broaden the EAB, the overall effect on bandwidth is limited. For example, increasing h_1 from 1 mm to 3 mm only expands the EAB from 13.71 GHz to 14.32 GHz, an increment of just 0.61 GHz.

Nonetheless, layer thickness variations significantly affected absorption peak intensity, and these influences differed among layers (Figure 8). Specifically, increasing h_1 consistently reduces the overall peak RL. For h_2, the absorption peaks at low and high frequencies gradually decrease, whereas the mid-frequency absorption peak initially intensifies and then weakens, reaching a maximum absorption of −50.96 dB at a h_2 of 3 mm. The layer thickness h_3 exhibits its strongest absorption peak (−59.65 dB) at the intermediate frequency when set to 2.5 mm. Finally, when h_4 was set to 2.5 mm, the metastructure achieves a maximum peak absorption of −57.78 dB in the mid-to-high frequency range.

In summary, adjusting individual layer thicknesses primarily impacts the absorption peak positions and intensities rather than significantly altering the total effective bandwidth. Therefore, precise tuning of h_1 through h_4 is vital for optimizing the metastructure's microwave absorption performance across the desired frequency bands.

3.3. Microwave absorption mechanisms of the sunflower-inspired metastructure

The previous analysis revealed that increasing the ΔZ between adjacent layers narrows the EAB at lower frequencies (Figure 7). This is primarily attributed to local impedance mismatches introduced by the centrosymmetric configuration of the sunflower-inspired metastructure unit. To quantitatively analyze this effect, the effective input impedance (Z_{eff}) was calculated as follows:[32,33]

$$Z_{eff} = \sqrt{\frac{(1+S_{11})^2 - S_{21}^2}{(1-S_{11})^2 - S_{21}^2}} \quad \text{(XI)}$$

where S_{11} is the reflection coefficient and S_{21} is the transmission coefficient. Due to the presence of a copper foil backplane, transmission is suppressed ($S_{21} = 0$). Using the optimal structural parameters identified in Section 3.2, the computed real and imaginary parts of Z_{eff} are shown in

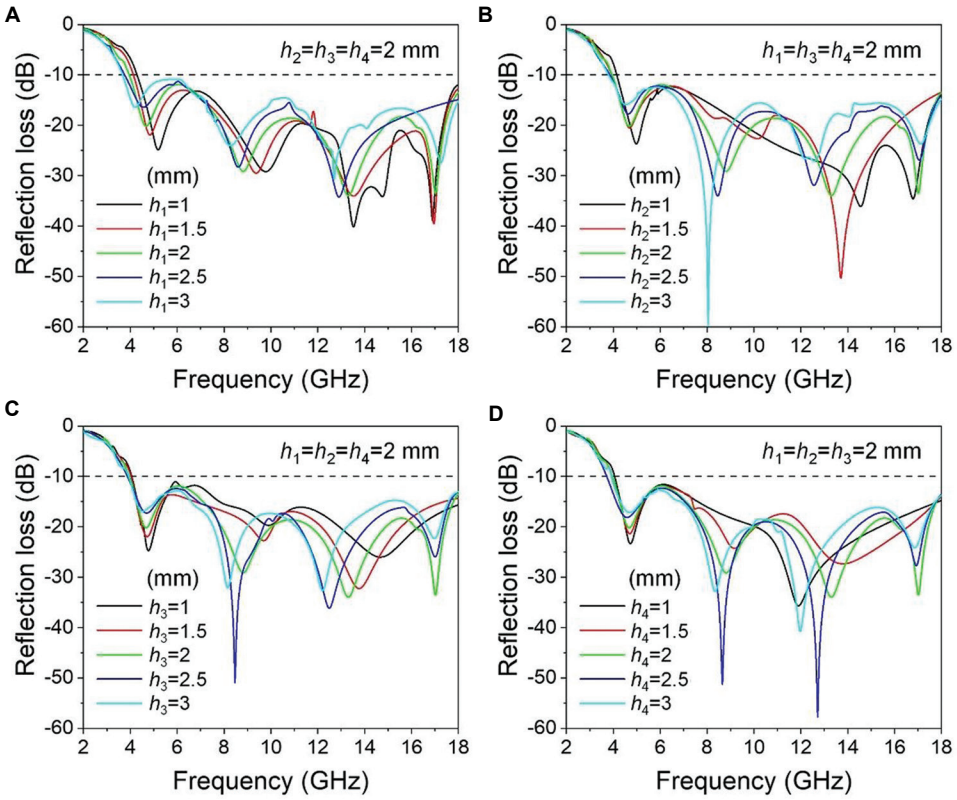

Figure 8. Effects of individual layer thickness on the absorption performance of the sunflower-inspired metastructure: (A) h_1, (B) h_2, (C) h_3, and (D) h_4

Figure 9. For effective absorption, Z_{eff} should closely match the impedance of free space, i.e., the real part should be close to 1, and the imaginary part close to 0. This condition is generally met above 3.93 GHz. However, in the 2 – 3.93 GHz range, both the real and imaginary parts fluctuate, indicating impedance mismatch and reduced absorption efficiency at low frequencies.

To further explore the metastructure's angular and polarization stabilities, RL was simulated under varying incident angles for both transverse electric (TE) and transverse magnetic (TM) polarizations. As shown in Figure 10, the metastructure maintains robust absorption performance across a range of incident angles. Under TE polarization, the EAB (RL < −10 dB) remains nearly unchanged up to 33°, due to enhanced multiple reflections and edge scattering between adjacent units.[34,35] Beyond 33°, the bandwidth gradually decreases as more waves are reflected at higher incident angles. TM polarization demonstrates greater angular stability. Even at 50°, the EABs for TE and TM waves remain as high as 10.63 GHz and 13.70 GHz, respectively. The centrosymmetric design of the metastructure unit also ensures polarization insensitivity, as confirmed by the consistent response at various polarization angles ranging from 0° (TE mode) to 90° (TM mode) in Figure 11.

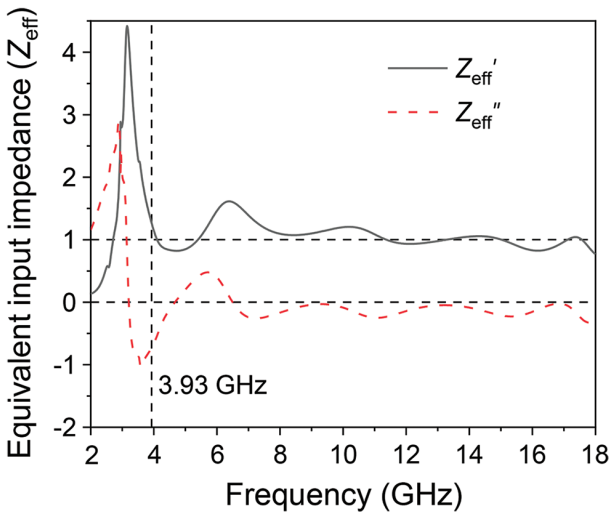

Figure 9. Real (Z_{eff}') and imaginary (Z_{eff}") parts of the equivalent input impedance (Z_{eff}) for the sunflower-inspired metastructure as a function of frequency, illustrating the impedance matching behavior with free space

To elucidate the absorption mechanisms, electric and magnetic field distributions were simulated at four characteristic peak frequencies: 4.66 GHz, 8.80 GHz, 13.25 GHz, and 17.04 GHz (Figure 12). At the first

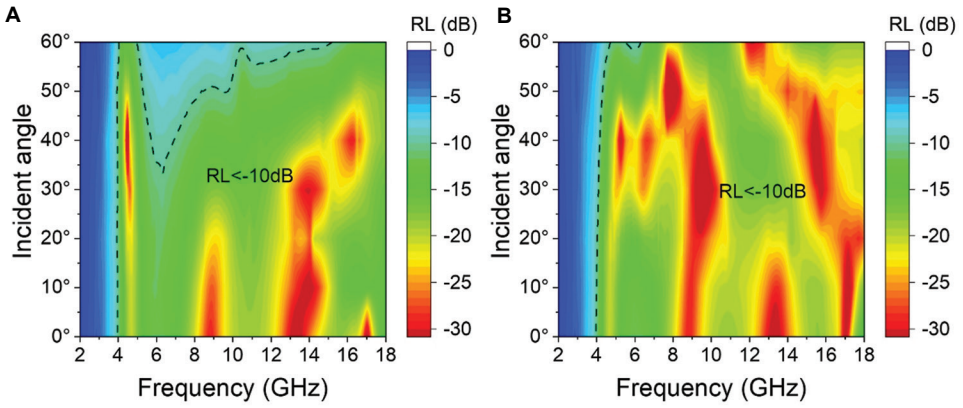

Figure 10. Absorption spectra of the sunflower-inspired metastructure under various incident angles and polarization states. (A) Reflection loss (RL) under transverse electric polarization for incident angles 0 – 60°. (B) RL under transverse magnetic polarization

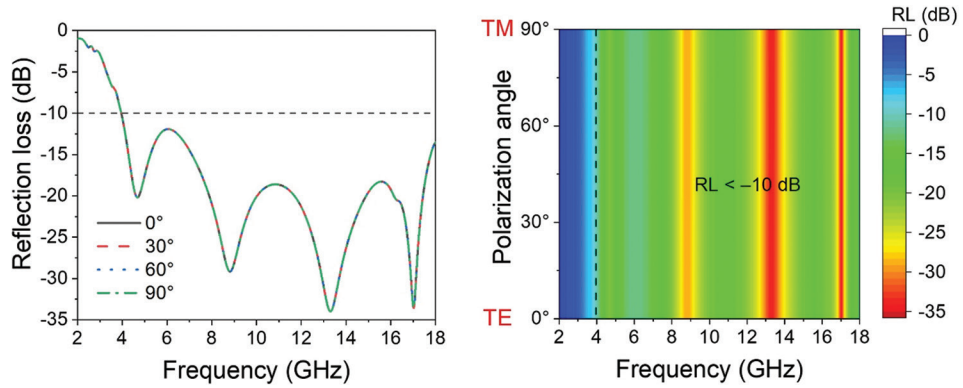

Figure 11. Polarization dependence of the sunflower-inspired metastructure, showing RL as a function of polarization angle and demonstrating polarization insensitivity
Abbreviations: TE: Transverse electric; TM: Transverse magnetic; RL: Reflection loss

peak frequency (4.66 GHz), the electric field mainly concentrates on the upper edges and inter-unit gaps, whereas the magnetic field localizes near the bottom metal plane, demonstrating a classic $\lambda/4$ resonance behavior.[36-38] At the second peak (8.80 GHz), the electric field extends to the top structure and across interlayer gaps, whereas the magnetic field shifts to the middle and lower sections of the absorber. By the third peak (13.25 GHz), a strong structural resonance appears between adjacent units, and the magnetic field shifts toward the top center. At the fourth peak (17.04 GHz), both electric and magnetic fields are concentrated near the top edge, exhibiting pronounced edge diffraction effects.[39,40]

Figure 13 presents the power loss density distributions at the same frequencies. At 4.66 GHz, energy loss is concentrated in the central region of the metastructure. As frequency increases, the loss region gradually shifts toward the top and eventually to the top edge. The loss culminates at the top edge by 17.04 GHz with strong energy dissipation at the structure's boundary, consistent with high-frequency edge diffraction effects.

In summary, the sunflower-inspired metastructure achieved microwave attenuation through multiple mechanisms:

- Low frequencies: $\lambda/4$ resonance induced by magnetic losses near the metal backplane;
- Intermediate frequencies: structural resonance between adjacent spiral layers;
- High frequencies: edge diffraction and strong field localization at the structure's periphery.

The correlation between the magnetic field and power loss distributions at high frequencies also suggests that magnetic losses, such as those caused by domain wall motion and hysteresis between adjacent structural units, are significant contributors to microwave absorption in the designed metastructure.

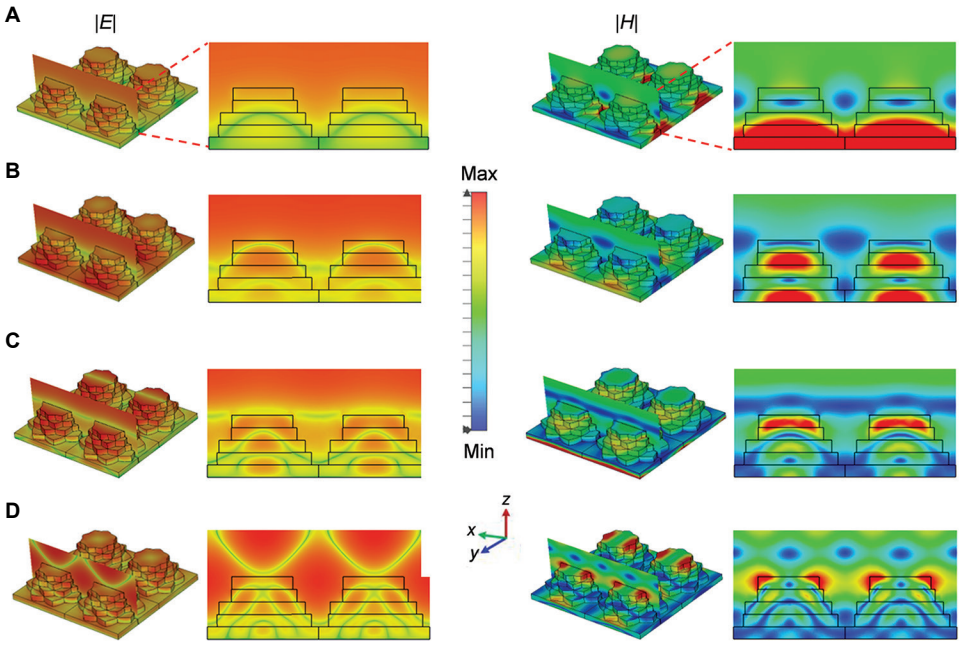

Figure 12. Simulated electric field (|*E*|, left) and magnetic field (|*H*|, right) distributions of the sunflower-inspired metastructure at absorption peak frequencies: (A) 4.66 GHz, (B) 8.80 GHz, (C) 13.25 GHz, and (D) 17.04 GHz, illustrating the evolution of the field localization and resonance behavior

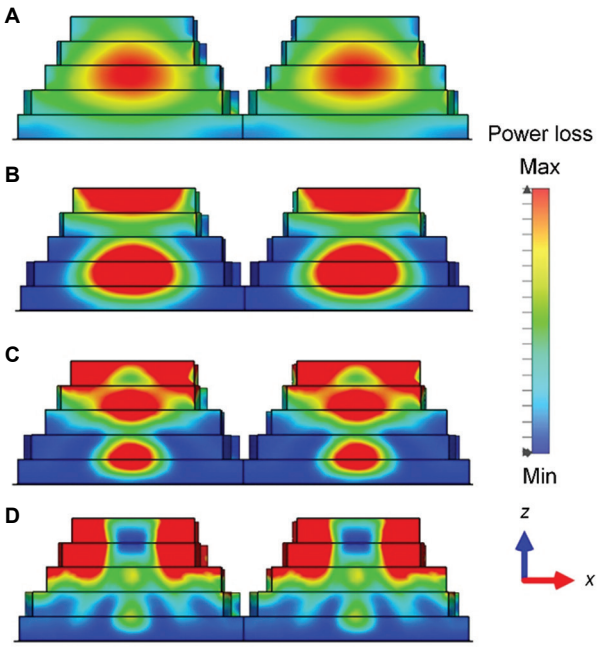

Figure 13. Simulated power loss density distributions of the metastructure at varying absorption peak frequencies: (A) 4.66 GHz, (B) 8.80 GHz, (C) 13.25 GHz, and (D) 17.04 GHz, showing the shift of energy dissipation from the structure's center to its top edge at higher frequencies

3.4. Experimental verification

To validate the accuracy and reliability of the simulation results, the sunflower-inspired metastructure was fabricated using FDM 3D printing, as shown in Figure 3. The simulated and experimentally measured RL curves at the incident angle of 0° under TE polarization are compared in Figure 14. Overall, the measured results exhibit a trend consistent with the simulations, confirming the validity of the electromagnetic modeling approach. However, minor discrepancies are observed between the measured and simulated data. These deviations are primarily attributed to several factors: the small unit size, dimensional inaccuracies, slight warping at the base of the printed sample, and surface roughness caused by the step effect inherent to the FDM process. These imperfections can lead to additional electromagnetic wave scattering and, consequently, diminished absorption efficiency.

The measured EAB (12.13 GHz) spans from 5.87 to 18 GHz, which is slightly narrower than the simulated bandwidth. In the 2 – 5.87 GHz range, the measured RL does not reach −10 dB, unlike in simulations (Figure 14). This discrepancy is potentially due to differences in the incident angle. While simulations assumed normal incidence, the experimental setup employed side-by-side horn antennas, resulting in a non-zero incident angle and reduced absorption. Nonetheless, the metastructure still demonstrates strong performance, maintaining over 80% absorptivity (i.e., RL < −7 dB) in the 3.16 – 5.87 GHz band.

In summary, the experimental findings validated the sunflower-inspired metastructure's excellent broadband microwave absorption performance. In addition, Table 2 compares the performance of this metastructure with

Table 2. Comparison of microwave absorption performance parameters between the sunflower-inspired metastructure and previously reported biomimetic microwave absorbers

Material	Structure	Thickness (mm)	Absorption bandwidth (GHz)	References
ABS	Bio-inspired gyroid	15	2.3 – 40	22
PEEK/FCIPs	Bamboo	15	3.2 – 40	17
Resistance patch+PLA	Honeycomb	15.51	3.53 – 24	19
Graphite powder/epoxy resin	Bio-inspired moth eye	20	5 – 18	23
CB-CIP/PLA	Sunflower-inspired metastructure	10	5.87 – 18	This study

Abbreviations: ABS: Acrylonitrile butadiene styrene; CB-CIP/PLA: Carbon black-carbonyl iron powder/polylactic acid; PEEK/FCIPs: Polyether ether ketone/flaky carbonyl iron powder.

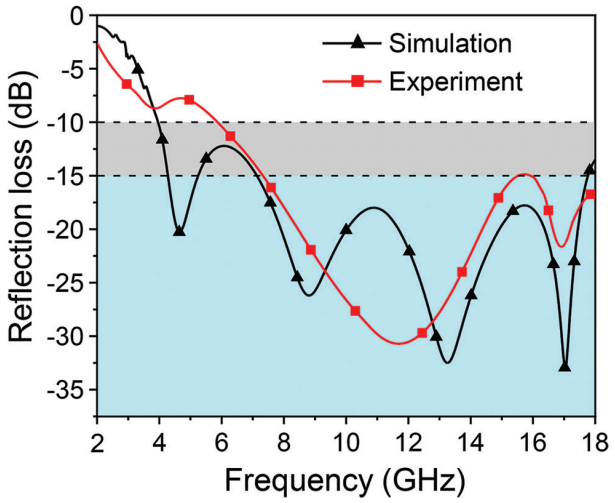

Figure 14. Comparison of simulated and experimentally measured reflection loss for the sunflower-inspired metastructure, demonstrating the consistency between simulation and measurement results

previously reported biomimetic absorbers. The present design achieves competitive absorption performance while maintaining a thinner profile. Compared to other structures, this metastructure benefits from reduced thickness and optimized material selection, demonstrating significant advantages in practical application. Finally, the metastructure is based on a periodic array of identical unit cells, which can be readily expanded or reduced to accommodate different application requirements.

4. Conclusion

This work presents a bio-inspired metastructure based on the spiral geometry of sunflower seed arrangements, developed for broadband microwave absorption. The metastructure integrates a CB-CIP/PLA composite and a multi-layered spiral gradient configuration to achieve both structural simplicity and enhanced electromagnetic performance. By optimizing structural parameters, particularly the gradient impedance increments between adjacent layers, a low-cost metastructure absorber was successfully fabricated using FDM 3D printing. Experimental results confirmed that the metastructure achieves an EAB of 12.13 GHz (5.87 – 18 GHz), with absorption rates exceeding 90% (RL < −10 dB), effectively covering the C, X, and Ku frequency bands.

In the CB-CIP/PLA composites used in this study, the interfacial polarization between CB and CIP improves the dielectric loss, while natural resonance enhances magnetic loss. These synergistic effects contribute to the efficient microwave attenuation observed. In addition, the metastructure absorber exhibits stable, wide-angle performance: for both TE and TM polarization states, the absorption bandwidths exceeding 10 GHz are maintained at incident angles up to 50°. Electric and magnetic field simulations, along with power loss density distributions, further confirmed the absorption mechanisms across different frequency bands, namely, $\lambda/4$ resonance at low frequencies, inter-layer structural resonance at intermediate frequencies, and edge diffraction at high frequencies. The findings demonstrate that combining biological inspiration with additive manufacturing offers a promising route for developing lightweight, efficient, and broadband microwave-absorbing materials.

Acknowledgments

None.

Funding

This study was funded by the Fuzhou–Xiamen–Quanzhou National Independent Innovation Demonstration Zone Collaborative Innovation Platform Project (3502ZCQXT2024003) and the Fujian Province Industry–University Cooperation Plan (2023H6015).

Conflicts of interest

The authors declare they have no competing interests.

Author's contributions

Conceptualization: Fei Wang, Kaiyong Jiang, Peifeng Li
Formal analysis: Pengfei Fang, Zhe Zhang

Funding acquisition: Fei Wang, Kaiyong Jiang
Investigation: Pengfei Fang, Fei Wang, Zhe Zhang
Methodology: Fei Wang, Kaiyong Jiang, Peifeng Li
Resources: Kaiyong Jiang
Validation: Fei Wang, Kaiyong Jiang, Peifeng Li
Writing–original draft: Pengfei Fang, Fei Wang
Writing–review & editing: Peifeng Li

Ethics approval and consent to participate

Not applicable.

Consent for publication

Not applicable.

Availability of data

The raw/processed data required to reproduce these findings cannot be shared at this time, as the data are part of an ongoing study.

References

1. Abdalla I, Cai JY, Lu W, Yu JY, Li ZL, Ding B. Recent progress on electromagnetic wave absorption materials enabled by electrospun carbon nanofibers. *Carbon.* 2023;213:118300.

   doi: 10.1016/j.carbon.2023.118300

2. Chen XT, Wu Y, Gu WH, *et al.* Research progress on nanostructure design and composition regulation of carbon spheres for the microwave absorption. *Carbon.* 2022;189:617-633.

   doi: 10.1016/j.carbon.2021.12.100

3. Li B, Liu M, Zhong W, *et al.* Partially contacted NixSy@N, S-codoped carbon yolk-shelled structures for efficient microwave absorption. *Carbon.* 2021;182:276-286.

   doi: 10.1016/j.carbon.2021.05.057

4. Guan X, Yang Z, Zhou M, *et al.* 2D MXene nanomaterials: Synthesis, mechanism, and multifunctional applications in microwave absorption. *Small Struct.* 2022;3(10):2200102.

   doi: 10.1002/sstr.202200102

5. Zhou W, Long L, Bu G, Li Y. Mechanical and microwave-absorption properties of Si3N4 ceramic with SiCNFs fillers. *Adv Eng Mater.* 2019;21(5):1800665.

   doi: 10.1002/adem.201800665

6. Houbi A, Aldashevich ZA, Atassi Y, Telmanovna ZB, Saule M, Kubanych K. Microwave absorbing properties of ferrites and their composites: A review. *J Magn Magn Mater.* 2021;529:167839.

   doi: 10.1016/j.jmmm.2021.167839

7. Jang W, Mallesh S, Lee S, Kim KH. Microwave absorption properties of core-shell structured FeCoNi@PMMA filled in composites. *Curr Appl Phys.* 2020;20(4):525-530.

   doi: 10.1016/j.cap.2020.01.019

8. Wang F, Zhou Q, Zhang Z, He P, Zhang J, Jiang K. Microwave absorption performance of carbon black/polylactic acid composite for fused filament fabrication. *Appl Sci Basel.* 2022;12(24):12747.

   doi: 10.3390/app122412747

9. Wang F, Zhou Q, Liu H, Fang P, Jiang K, Li P. Wide-angle broadband metamaterial absorber with carbon black-carbonyl iron/polylactic acid composites fabricated by fused filament fabrication. *Mater Sci Addit Manuf.* 2024;3(3):4158.

   doi: 10.36922/msam.4158

10. Ding GX, Chen CX, Tai HX, *et al*. Structural characterization and microwave absorbing performance of CuFe2O4/RGO composites. *J Solid State Chem.* 2021;297:22051.

    doi: 10.1016/j.jssc.2021.122051

11. Zhang K, Gao X, Zhang Q, Chen H, Chen X. Fe3O4 nanoparticles decorated MWCNTs @ C ferrite nanocomposites and their enhanced microwave absorption properties. *J Magn Magn Mater.* 2018;452:55-63.

    doi: 10.1016/j.jmmm.2017.12.039

12. Ding DH, Luo F, Zhou WC, Shi YM, Zhou L. Research status and outlook of high temperature radar absorbing materials. *J Inorg Mater.* 2014;29(5):461-469.

    doi: 10.3724/sp.J.1077.2014.13471

13. Tang XJ, Li XB, Sun HG. Preparation and Properties of an Anti-Friction and Anti-Corrosive Radar Absorbing Material with Periodic Intermediate Coating. In: *Paper Presented at: 6th Annual International Conference on Material Science and Environmental Engineering (MSEE),* Chongqing, PR China; 2018.

    doi: 10.1088/1757-899x/472/1/012012

14. Wang YM, Pan M, Liang XY, Li BJ, Zhang S. Electromagnetic wave absorption coating material with self-healing properties. *Macromol Rapid Commun.* 2017;38(23):1700447.

    doi: 10.1002/marc.201700447

15. Li AB, Zhao XG, Duan GW, Anderson S, Zhang X. Diatom frustule-inspired metamaterial absorbers: The effect of hierarchical pattern arrays. *Adv Funct Mater.* 2019;29(22):1809029.

    doi: 10.1002/adfm.201809029

16. Lopez-Garcia M, Masters N, O'Brien HE, *et al*. Light-induced dynamic structural color by intracellular 3D photonic crystals in brown algae. *Sci Adv.* 2018;4(4):eaan8917.

    doi: 10.1126/sciadv.aan8917

17. Duan Y, Liang Q, Yang Z, *et al*. Bamboo-inspired composite metastructure for broadband microwave absorption and

load bearing. *Mater Res Bull.* 2023;166:112368.

doi: 10.1016/j.materresbull.2023.112368

18. Huang L, Duan Y, Dai X, *et al*. Bioinspired metamaterials: Multibands electromagnetic wave adaptability and hydrophobic characteristics. *Small.* 2019;15(40):1902730.

doi: 10.1002/smll.201902730

19. Jiang W, Yan LL, Ma H, *et al*. Electromagnetic wave absorption and compressive behavior of a three-dimensional metamaterial absorber based on 3D printed honeycomb. *Sci Rep.* 2018;8:4817.

doi: 10.1038/s41598-018-23286-6

20. Huang L, Duan Y, Liu J, *et al*. Bionic composite metamaterials for harvesting of microwave and integration of multifunctionality. *Compos Sci Technol.* 2021;204:108640.

doi: 10.1016/j.compscitech.2020.108640

21. Wu W, Xu R, Zhou Y, *et al*. Biomimetic 3D coral reef-like GO@TiO2 composite framework inlaid with TiO2-C for low-frequency electromagnetic wave absorption. *Carbon.* 2021;178:144-156.

doi: 10.1016/j.carbon.2020.11.085

22. An Q, Li DW, Liao WH, *et al.* A novel ultra-wideband electromagnetic-wave-absorbing metastructure inspired by bionic gyroid structures. *Adv Mater.* 2023;35(26):2300659.

doi: 10.1002/adma.202300659

23. Chen ZM, Zhang Y, Wang ZD, *et al.* Bioinspired moth-eye multi-mechanism composite ultra-wideband microwave absorber based on the graphite powder. *Carbon.* 2023;201:542-548.

doi: 10.1016/j.carbon.2022.09.035

24. Chen X, Li YL, Cheng SY, *et al.* Liquid metal-MXene-based hierarchical aerogel with radar-infrared compatible camouflage. *Adv Funct Mater.* 2024;34(10):2308274.

doi: 10.1002/adfm.202308274

25. Chen Y, He YQ, Zhu XQ. Flower-type pulsating heat pipe for a solar collector. *Int J Energy Res.* 2020;44(9):7734-7745.

doi: 10.1002/er.5505

26. Xu YC, Huang YZ, Yan H, *et al*. Sunflower-pith-inspired anisotropic auxetic mechanics from dual-gradient cellular structures. *Matter.* 2023;6(5):1569-1584.

doi: 10.1016/j.matt.2023.03.010

27. Yu SQ, Liu JG, Zhao PY, Tang YY. A flat-foldable equiangular spiral folding pattern inspired by sunflowers for deployable structures. *Chin J Aeronaut.* 2024;37(6):425-438.

doi: 10.1016/j.cja.2023.10.004

28. Wang F, Zhou QF, Zhang Z, Gu YH, Zhang JL, Jiang KY. Microwave absorption properties of carbon black-carbonyl iron/polylactic acid composite filament for fused deposition modeling. *Materials.* 2022;15(15):5455.

doi: 10.3390/ma15155455

29. Feng MF, Zhang KF, Xiao JJ, *et al.* Material-structure collaborative design for broadband microwave absorption metamaterial with low density and thin thickness. *Compos Pt B-Eng.* 2023;263:110862.

doi: 10.1016/j.compositesb.2023.110862

30. Lei L, Yao ZJ, Zhou JT, Wei B, Fan HY. 3D printing of carbon black/polypropylene composites with excellent microwave absorption performance. *Compos Sci Technol.* 2020;200:108479.

doi: 10.1016/j.compscitech.2020.108479

31. Ye XC, Yang C, He EY, *et al.* Electromagnetic wave absorption properties of the FeSiAl/PLA and FeSiAl-MoS2-Graphene/PLA double-layer absorber formed by fused deposition modeling. *J Magn Magn Mater.* 2023;565:170280.

doi: 10.1016/j.jmmm.2022.170280

32. Baqir MA, Latif H, Altintas O, *et al*. Fractal metamaterial based multiband absorber operating in 5G regime. *Optik.* 2022;266:169626.

doi: 10.1016/j.ijleo.2022.169626

33. Zhang Z, Wang F, Zhang JL, Li PF, Jiang KY. Ultra-broadband and wide-angle metamaterial absorber with carbon black/carbonyl iron composites fabricated by direct-ink-write 3D printing. *Adv Eng Mater.* 2023;25(6):2201236.

doi: 10.1002/adem.202201236

34. Min DD, Zhou WC, Qing YC, Luo F, Zhu DM. Single-layer and double-layer microwave absorbers based on graphene nanosheets/epoxy resin composite. *Nano.* 2017;12(7):1750089.

doi: 10.1142/s1793292017500898

35. Zhou Q, Yin XW, Ye F, Liu XF, Cheng LF, Zhang LT. A novel two-layer periodic stepped structure for effective broadband radar electromagnetic absorption. *Mater Des.* 2017;123:46-53.

doi: 10.1016/j.matdes.2017.03.044

36. Duan YB, Liang QX, Yang Z, et al. A wide-angle broadband electromagnetic absorbing metastructure using 3D printing technology. *Mater Des.* 2021;208:109900. doi: 10.1016/j.matdes.2021.109900

37. Huang YX, Song WL, Wang CX, *et al*. Multi-scale design of electromagnetic composite metamaterials for broadband microwave absorption. *Compos Sci Technol.* 2018;162:206-214.

doi: 10.1016/j.compscitech.2018.04.028

38. Wang BC, Wei JQ, Yang Y, Wang T, Li FS. Investigation on peak frequency of the microwave absorption for carbonyl iron/epoxy resin composite. *J Magn Magn Mater.* 2011;323(8):1101-1103.

doi: 10.1016/j.jmmm.2010.12.028

39. Fan QF, Huang YX, Chen MJ, Li Y, Song WL, Fang DN. Integrated design of component and configuration for a flexible and ultrabroadband radar absorbing composite. *Compos Sci Technol.* 2019;176:81-89.

doi: 10.1016/j.compscitech.2019.04.008

40. Ning J, Dong SF, Luo XY, *et al.* Ultra-broadband microwave absorption by ultra-thin metamaterial with stepped structure induced multi-resonances. *Results Phys.* 2020;18:103320.

doi: 10.1016/j.rinp.2020.103320